

Atomistic Simulation of Alkanethiol Self-Assembled Monolayers on Different Metal Surfaces via a Quantum, First-Principles Parametrization of the Sulfur–Metal Interaction

Orestis Alexiadis,^{†,‡,§} Vagelis A. Harmandaris,^{*,†} Vlasis G. Mavrantzas,^{‡,§} and Luigi Delle Site^{*,†}

Max Planck Institute for Polymer Research, D-55128, Mainz, Germany, Department of Chemical Engineering, University of Patras, GR 26504, Patras, Greece, and Institute of Chemical Engineering and High Temperature Chemical Processes (FORTH-ICE/HT), GR 26504, Patras, Greece

Received: November 7, 2006; In Final Form: February 14, 2007

A detailed investigation of the effect of the substrate on the structure and conformation of alkanethiol self-assembled monolayers is presented through detailed atomistic simulations based on a first-principles density functional modeling of the sulfur–metal interaction. Ab initio calculations on a methanethiol molecule adsorbed on different metal surfaces (gold, silver, and platinum) are conducted, and the data obtained are used to develop an accurate classical force field for the sulfur–metal interaction. This serves as input to a very efficient Monte Carlo algorithm with which detailed atomistic simulations are carried out with a number of model alkanethiol self-assembled monolayers (SAMs) adsorbed on the three different substrates. Emphasis is given primarily to the study of the effect of the substrate on the structural properties of the simulated alkanethiol SAMs, such as molecular orientation, molecular conformation, and statistics of gauche defects, as a function of their chain length.

A. Introduction

The spontaneous adsorption of relatively short molecules (10–20 methylene groups) of the alkane class onto metal surfaces, through the replacement of the terminal methyl (R- or -CH₃) group with a functional group (e.g., a mercaptan group, -SH), leads to R–SH systems with well-defined structures, the so-called self-assembled monolayers (SAMs) whose novel properties render them very useful in many applications.^{1,2} Alkanethiol-based SAMs on the Au(111) surface, in particular, are commonly used as a prototypical model in experiments^{3–11} for studying specific structural features of monomolecular films and how chemical alterations in the chain backbone and/or the terminal group affect the structure of the formed film. Unfortunately, despite the extensive literature on the properties of organosulfur adsorbents (especially thiolates) on the Au(111) metal substrate, little is known about the formation of alkanethiol-based SAMs on the Ag(111) surface, and even less on the Pt(111) one. For example, despite the similarities of Au(111) and Ag(111) substrates (same symmetry, similar lattice spacing, etc.), alkanethiol films formed on an Ag(111)¹² surface display significant differences compared to the R–SH/Au(111) systems, such as a different packing of the S atoms: in the case of the Ag(111) surface, this is described as $(\sqrt{7} \times \sqrt{7})R10.9^\circ$, as compared to the $(\sqrt{3} \times \sqrt{3})R30^\circ$ packing on Au(111) with a S–S spacing of 4.41 Å as observed for a chemisorbed methylthiolate by SFG spectroscopy (see parts a and b of Figure 1).¹² However, for larger molecular systems, such as CH₃(CH₂)₉S and CH₃(CH₂)₁₇S, He and GIX

diffraction as well as STM studies have indicated a lattice constant of 4.6–4.8 Å and an overlayer similar to the $(\sqrt{7} \times \sqrt{7})R10.9^\circ$ one, but with two domains rotated by $\sim 24^\circ$ with respect to each other ($\sim 12^\circ$ with respect to the Ag(111) plane rather than 10.9°).^{13,14} Because of the difference in the S–S distance, it is expected that thiolate monolayers on Ag(111) are more densely packed than those on Au(111), which should generally result in smaller tilt angles. (See Figure 2 for a schematic description of the angles characterizing the R–SH chain backbone structure). Indeed, although the range of reported values for the tilt angle of an alkanethiol on an Ag(111) surface ranges from 0 to 14° ,^{8,13} the consensus is that in an R–SH/Ag(111) SAM the thiolate chains are practically standing normal to the Ag substrate.

Contrary to the Ag surface, adsorption of alkanethiol monolayers on Pt has not been studied extensively and little is known about the structure and properties of the corresponding thiol-based SAMs. It has been found that the chemisorption of a methanethiol on a Pt(111) substrate at room temperature (298 K) leads to a $(\sqrt{3} \times \sqrt{3})R30^\circ$ pattern with the S atoms occupying the threefold hollow fcc sites and the C ones residing above the hcp threefold sites.¹⁵ The same structure has been observed for a number of larger alkanethiol molecules (1-hexanethiol and 1-nonanethiol) as well as for benzenethiol ones, with a value of the S–S lattice spacing in the latter ca. 4.8 Å.¹⁶

From the point of view of molecular simulations, attention has been paid mainly to the investigation of structural properties and domain formation of thiol-based SAMs formed on a Au(111) surface. From the molecular point of view, the formation of the monolayer and its highly ordered structure are governed by mechanisms involving a number of complicated interactions, such as sulfur–metal chemical bonding, van der Waals interactions, entropy loss of the adsorbed chains, hindered chain and segmental mobility, and thermal effects. To elucidate them,

* Authors to whom correspondence should be addressed. E-mail: harmanda@mpip-mainz.mpg.de; dellsite@mpip-mainz.mpg.de.

[†] Max Planck Institute for Polymer Research.

[‡] University of Patras.

[§] Institute of Chemical Engineering and High Temperature Chemical Processes.

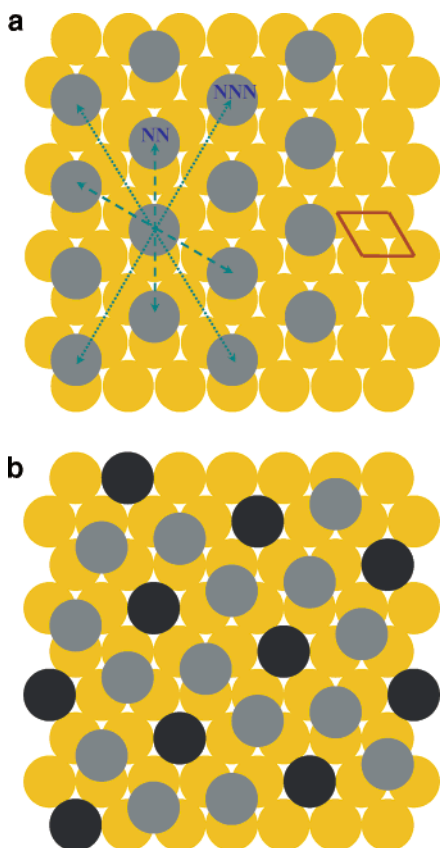


Figure 1. (a) Sketch of the $(\sqrt{3} \times \sqrt{3})R30^\circ$ lattice formed by S atoms (gray circles) occupying the threefold sites of an ideal Au(111) substrate (yellow circles). The vectors represent the nearest-neighbor (NN) (dashed lines) and next-nearest-neighbor (NNN) (dotted lines) directions. The unit cell of the Au(111) plane is also shown with the thick solid orange lines. (b) Sketch of the $(\sqrt{7} \times \sqrt{7})R10.9^\circ$ structure. Yellow circles represent the Ag atoms, while the black and gray circles represent the S atoms residing on the top and threefold hollow sites, respectively.

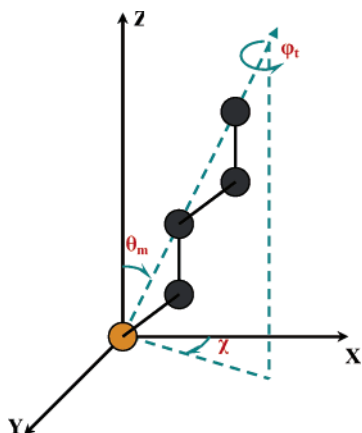


Figure 2. Schematic illustration of the angles defining the orientation of an adsorbed alkanethiol molecule: θ_m is the tilt angle of the chain, ϕ_t is the twist angle for rotation about the chain axis, and χ is the tilt direction (precession) angle.

various models and approximations have been proposed and a number of atomistic molecular dynamics (MD)^{17–21} and Monte Carlo (MC)^{22,23} simulations have been carried out addressing aspects related mainly to the bonding of the S atoms on the Au surface and the thermal behavior of the monomolecular film. In the majority of the cases, these simulations were started from an initial configuration where the initial setup of the system

was presumed; the S atoms were arranged in a $(\sqrt{3} \times \sqrt{3})R30^\circ$ hexagonal lattice, and the molecules adopted an all-trans configuration with the planes of the C backbones in a herringbone arrangement. This issue was addressed only very recently through the development of an efficient MC algorithm capable of driving a random configuration of a system of alkanethiol molecules to the Au(111) surface, thus leading to a highly ordered final structure representative of the monolayer formed in an actual experiment irrespective of the initial setup.²⁴

In addition to classical simulations, first-principles (ab initio) calculations have been carried out in order to clarify aspects of the chemisorption of alkanethiols on different metal substrates concerning, for example, the geometry and energetics of the sulfur–metal bonding.^{25–29} Through fits to an empirical potential, these ab initio calculations can further provide the necessary data for subsequent use in MD simulations.^{30–32} On the basis of this idea, we present here results from classical simulations in which a quantum-based, first-principles parametrization of the sulfur–metal interaction was utilized. This methodology allowed us to investigate the interaction of alkanethiol SAMs with different metal surfaces, beyond the well-studied R–SH/Au(111) system. The approach entails the development of an accurate classical force field for the description of the interactions of alkanethiol molecules with the considered metal surface, using data provided by Car–Parrinello MD calculations.²⁹ This force field is next used as input in the recently proposed atomistic MC algorithm,²⁴ and predictions are made for the structural properties of the simulated bulk multichain system through detailed atomistic-level simulations. This has allowed us to study the structure of adsorbed alkanethiol chains on three different metal surfaces (Au, Ag, and Pt), and its dependence on chain length. The novelty of this modeling approach entails in the systematic investigation of the effect of the substrate on the structure of the formed monolayer and the different degrees of chain organization that can be achieved by switching from one substrate to another.

The paper is organized as follows: Section B discusses details of the simulation technique (simulation tools used in the work and description of the force field development). Results concerning the structure of a number of alkanethiol SAMs characterized by different chain lengths on the three metal surfaces are presented in section C. The paper concludes with section D summarizing the most important results of the work.

B. Simulation Methodology

1. Ab Initio First-Principle Calculations. The ab initio (first-principles) calculations were performed with a $\text{CH}_3\text{--S}$ molecule adsorbed on the (111) planes of a Au, Ag, or Pt surface,²⁹ and allowed us to extract information about the favorable adsorption sites for each surface, the strength of the sulfur–surface bonding (adsorption energy), and its geometrical characteristics. They were carried out with the density-functional-based finite-electronic temperature method (FEMD)³³ implemented in the plane-wave-based CPMD code.³⁴ In this method, the electron density and the Hellmann–Feynman forces are determined via a subspace diagonalization of the high-temperature electron density matrix. The subspace was expanded in a plane-wave basis set with a cutoff of 60 Ry (this turned out to be sufficient after test runs using higher cutoff values, up to 90 Ry). We employed norm-conserving-type pseudopotentials, generated according to the Troullier–Martins scheme, except for S where we made use of a Goedecker-type. All of the pseudopotentials were accurately tested to provide correct predictions of the bulk and surface properties of the metals, and of the structural

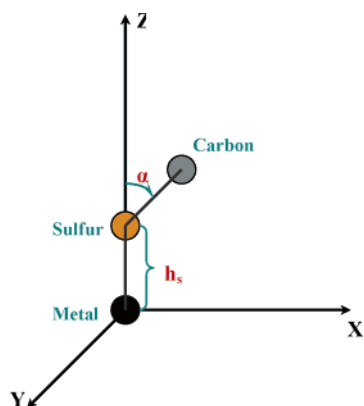


Figure 3. Drawing of the metal–S–CH₂ angle α and the minimum distance, h_s , of the S atom from the surface, as defined in the ab initio (first principles) calculations with the adsorbed CH₃–S molecule on the three surfaces.

TABLE 1: Data Acquired from the Ab Initio (First Principles) Calculations for the Stable Geometries of the CH₃–S Molecule Adsorbed on the (111) Planes of the Au, Pt, and Ag Surfaces^a

	Au	Pt	Ag
E_{ads} (kcal/mol)	−40.6 (fcc)	−61.8 (fcc)	−44.8 (fcc)
h_s (Å)	1.7	1.6	1.8
α (deg)	0.85	13.1	22.4

^a The favorable adsorption sites are given in brackets.

properties of the thiol molecule. The PBE generalized gradient approximation was also applied.³⁵

The prototype system consisted of a (111) surface, modeled with four layers with the bottom two being kept fixed during the geometry optimization process, and a methanethiol molecule, on which we carried out a full geometry optimization. We employed supercells of lateral dimensions corresponding to arrays of 3×3 atoms. Geometry optimizations were carried out at each high-symmetry site of the 111 surfaces (that is, atop, bridge, fcc hollow, and hcp hollow). For each site, several molecular orientations were considered as initial geometry and

the most stable one, after optimization of the whole structure, was used to model the adhesion of the molecule to the surface. For this work, in particular, only the data of the most stable configurations were used (see Table 1). A more detailed description of the ab initio study will be presented elsewhere.²⁹

2. Force Field Development. The second stage of our simulation approach refers to the development of an accurate classical force field for the sulfur–metal interaction. For this, we are using the data from the ab initio calculations, presented in the previous section. Our classical simulations use a flat surface model; that is, metal molecules are not explicitly present. The interaction of the substrate with the sulfur head group is considered as a function of two contributions; the first, $V(z)$, describes the z -dependence of the interaction between S and metal, while the second, $V_b(\alpha)$, describes interactions associated with the orientation of the molecule:

$$V_{\text{metal-sulfur}} = V(z) + V_b(\alpha) \quad (1)$$

The z -dependent distance potential, $V(z)$, is described by a 12–3 Lennard-Jones potential of the form

$$V(z) = \left(\frac{C_{12}}{z^{12}} \right) - \left(\frac{C_3}{z^3} \right) \quad (2)$$

where C_{12} and C_3 are parameters characterizing the strength of the potential. To calculate C_{12} and C_3 , we use the CPMD data about the adsorption energy, E_{ads} , of the methanethiol (CH₃–S) and the perpendicular distance, h_s , of the S atom from the surface from the ab initio calculations described in the previous section (see also Table 1). The values of the derived parameters are shown in Table 2. Note that E_{ads} is very high and $V(z)$ describes the S–metal bond. The $V_b(\alpha)$ term describes the orientation of the bond connecting the S atom with the first CH₂ group of the alkanethiol molecule with respect to the metal surface through the angle α (see Figure 3); the equilibrium value, α_0 , of this angle is directly available from the ab initio calculations with the CH₃S molecule (see Table 1). A harmonic potential is used to describe the thermal fluctuations associated with the metal–S–CH₂ angle, α

TABLE 2: Interaction Parameters of the Molecular Model Used in our Simulations

type of interaction and potential function	type of interacting sites								
bond-bending interactions $V_{\text{bend}}(\theta) = 1/2 k_b (\theta - \theta_0)^2$ θ_0 (deg) k_b (kcal mol ^{−1} rad ^{−2})	CH ₁ –CH ₂ –CH ₂ ($x = 2, 3$)			S–CH ₂ –CH ₂			metal–S–CH ₂		
	Au	Pt	Ag	Au	Pt	Ag	Au	Pt	Ag
				114.4	114.4	114.4	0	22	13
				124.2	124.2	124.2		124.2	
dihedral angle interactions $V_{\text{tor}}(\phi) = \sum_{i=0}^n \alpha_i \cos^i(\phi)$ α_i (kcal mol ^{−1})	X–CH ₂ –CH ₂ –CH ₂ ($X = \text{S, CH}_2, \text{CH}_3$)								
	$\alpha_0 = 2.217/\alpha_1 = 2.905/\alpha_2 = -3.135$ $\alpha_3 = -0.731/\alpha_4 = 6.271/\alpha_5 = -7.527$								
nonbonded interactions $V_{\text{LJ}}(r_{ij}) = 4\epsilon_{ij} [(\sigma_{ij}/r_{ij})^{12} - (\sigma_{ij}/r_{ij})^6]$ σ_{ij} (Å) ϵ_{ij} (kcal mol ^{−1})	Au	Ag	Pt	S–S	S–CH ₂	S–CH ₃	CH ₂ –CH ₂	CH ₂ –CH ₃	CH ₃ –CH ₃
	4.428	4.205	4.241	Au	Pt	Ag	Au	Pt	Ag
		0.2504		0.1719	0.2094	0.118	0.1437	0.1751	
atom–surface interactions $V_{\text{metal}} = C_{12}/z^{12} - C_3/z^3$ C_{12} (10 ⁴ kcal Å ^{−12} mol ^{−1}) C_3 (10 ² kcal Å ^{−3} mol ^{−1})	Au	Ag	Pt	S–metal	CH ₂ –metal	CH ₃ –metal	Au	Ag	Pt
	0.846	2.397	0.579	Ag	Pt	Ag	Au	Ag	Pt
	2.707	3.778	3.375		158.208	0.783		192.722	0.953

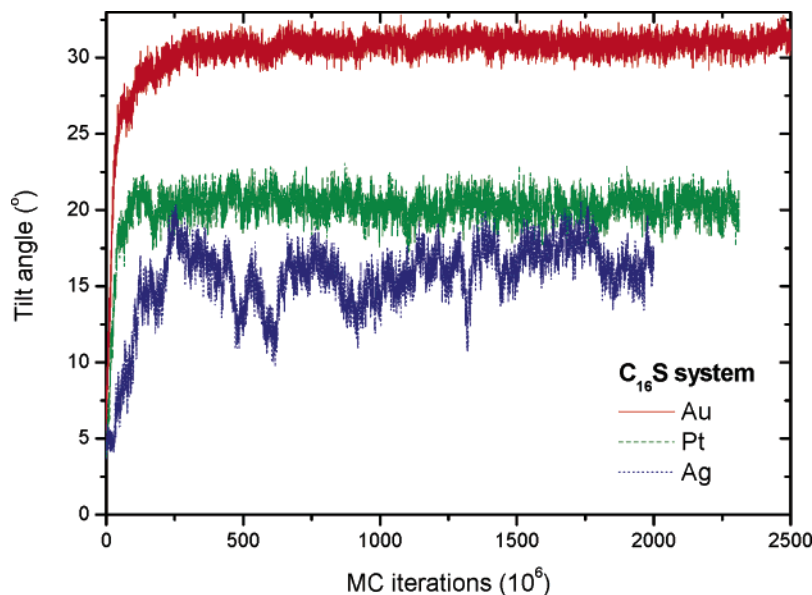


Figure 4. Time evolution (in MC iterations) of the tilt angle for the $C_{16}S$ system on the three metal substrates.

TABLE 3: Systems Studied and Simulation Details

simulation details and surface properties	systems simulated		
	$CH_3-(CH_2)_n-SH, n = 9, 15, 21$		
	Au	Pt	Ag
surface cell dimensions (\AA)	54.67×43.041	52.36×41.223	51.92×40.876
S–S lattice spacing (\AA)	4.97	4.76	4.72
temperature (K)	300	300	300
number of alkanethiol molecules	110	110	110

$$V_b(\alpha) = \frac{1}{2} k_b (\alpha - \alpha_0)^2 \quad (3)$$

where the constant k_b was chosen to be equal to that used to describe the interaction of the $CH_2-CH_2-CH_2$ bending angle (see Table 2). This (bending) potential is intended to describe all of the contributions from the interaction of the first CH_2 group with the metal surface; that is, the first CH_2 group is not interacting additionally with the substrate.

For the classical simulations, a united atom model was used, which distinguishes between three different types of atomistic units: methyl (CH_3), methylene (CH_2), and mercaptan (SH). The rest of the atomistic model includes the bonded and nonbonded interactions between interacting units and is based on the united atom representation of Hautman and Klein.¹⁷ The bonded part of the force field includes bond bending and dihedral angle interactions (bonds are kept fixed, equal to 1.84 and 1.53 \AA for the S–C and all C–C bonds, respectively), whereas the nonbonded interactions are described through a standard Lennard-Jones potential. As far as the CH_3 and CH_2 units are concerned, their interactions with the surface were described via a standard 12–3 Lennard-Jones potential with

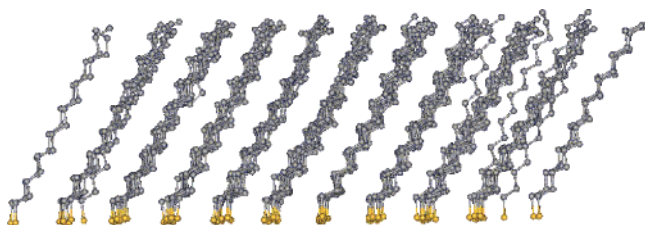


Figure 5. Final configuration of the $C_{16}S/Au$ system. The yellow spheres represent the S atoms, while the C atoms are depicted by dark-gray spheres.

parameters taken from the literature.¹⁷ Finally, to restrict the mobility of S atoms, which is quite high due to the flat surface model, and stabilize their spacing to its experimental value, a larger value (compared to the Hautman–Klein model) of the core size for the S–S interactions (different for each surface) was used.²² Note that the classical force field developed here is the first step in a hierarchical modeling scheme for the simulation of these highly organized systems, which combines quantum, first-principles calculations and classical simulations. It is also very promising that the results obtained about the structural properties of the formed SAMs (see the next section) are in very good qualitative and quantitative agreement with the available experimental data. However, the assumption of a flat surface model imposes certain limitations on the predictive capability of the model, especially for length scales down to one atomic diameter from the substrate ($\sim 2-3 \text{\AA}$). For this reason, in the future, a more detailed classical force field should be developed with individual metal molecules being explicitly taken into account. The possibility of sulfur atoms forming dimers on the metal surface should also be examined and analyzed by performing ab initio calculations with more than one CH_3-S molecule.

The values of all of the parameters of the developed classical force field are summarized in Table 2.

3. Atomistic Simulations and Systems Studied. To equilibrate the initial configurations of the alkanethiol molecules on the three metal surfaces and study their structural properties, MC simulations were carried out using the developed force field. The corresponding MC algorithm is based on the implementation of various, widely known moves, which were modified here to account for the different structural parameters along an alkanethiol chain. The MC moves employed in the atomistic simulations of the present study are the following:

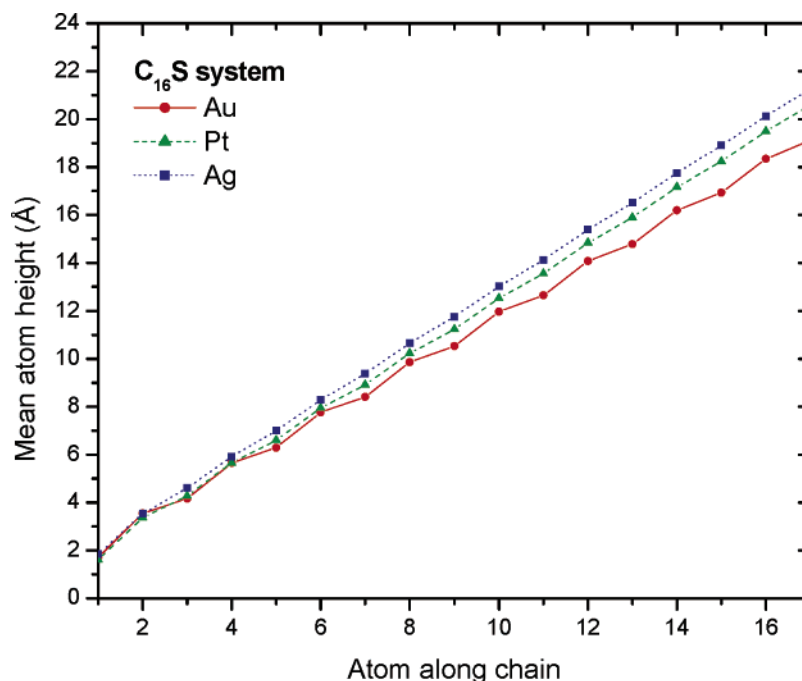


Figure 6. Results for the mean atom distance $\langle z \rangle$ along a $\text{CH}_3\text{-(CH}_2\text{)}_{15}\text{-SH}$ chain from the Au(111), Ag(111), and Pt(111) planes.

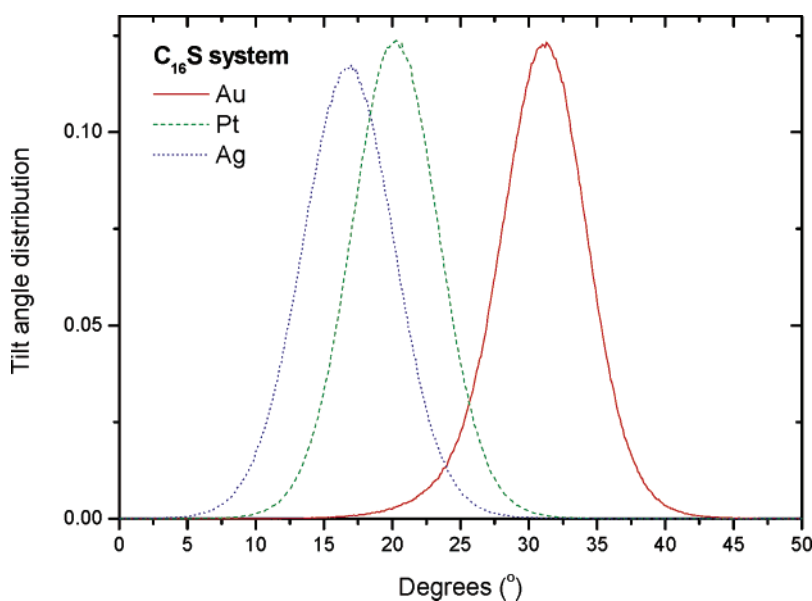


Figure 7. Normalized distributions of the molecular tilt angle, θ_m , in the $\text{C}_{16}\text{S/Au}$, $\text{C}_{16}\text{S/Pt}$, and $\text{C}_{16}\text{S/Ag}$ systems.

TABLE 4: Selected Results from the Monte Carlo Simulations

properties	simulated systems								
	Au			Pt			Ag		
	C_{10}S	C_{16}S	C_{22}S	C_{10}S	C_{16}S	C_{22}S	C_{10}S	C_{16}S	C_{22}S
$\langle z_{\text{tail}} \rangle$ (Å)	12.8 ± 0.17	19.1 ± 0.24	26 ± 0.31	13.8 ± 0.21	20.6 ± 0.24	27.3 ± 0.24	14.4 ± 0.14	21.3 ± 0.36	28 ± 0.22
experimental $\langle z_{\text{tail}} \rangle$ (Å)	12.5–15.6	18.0–22.0	24.0–32.0	13.6	21.4	29.2		21.5	
$\langle \theta_m \rangle$ (deg)	29.9 ± 2.0	30.9 ± 1.8	29.7 ± 1.6	17.1 ± 4.2	20.2 ± 3.0	22.2 ± 1.8	7.7 ± 3.3	16.8 ± 5.0	20.1 ± 1.8
$\langle \chi \rangle$ (deg)	11.9	14.1	24.0	16.7	22.1	23.5	14.6	18.8	23.6

(1) The *flip* move, which involves the rotation of an internal atom along an alkanethiol chain about the axis connecting the two atoms on the two sides of the selected atom, by altering the corresponding dihedral angle, (2) the *end atom rotation* move, which also consists of changes in the dihedral angle of a chain's end atom and its rotation about the axis of the bond prior to the last one, (3) the *configurational biased* (CCB) move, which involves the deletion of a number of monomers along an alkanethiol chain and a step-by-step regeneration of every

monomer in the cut segment in a biased fashion,^{36,37} (4) the *bias reptation* move, which is a variant of the *generalized reptation* move accounting for the sulfur atom. Upon selection of this move, the two end atoms (S, CH_3) along an alkanethiol chain are extracted and the CH_3 atom is regenerated in the place of S atom; at the same time, the type of the CH_3 atom is changed to CH_2 and the S atom is rebuilt over the new CH_2 monomer, and finally (5) the *concerted rotation* (CONROT) move,^{38,39} which involves removing a trimer of consecutive internal atoms

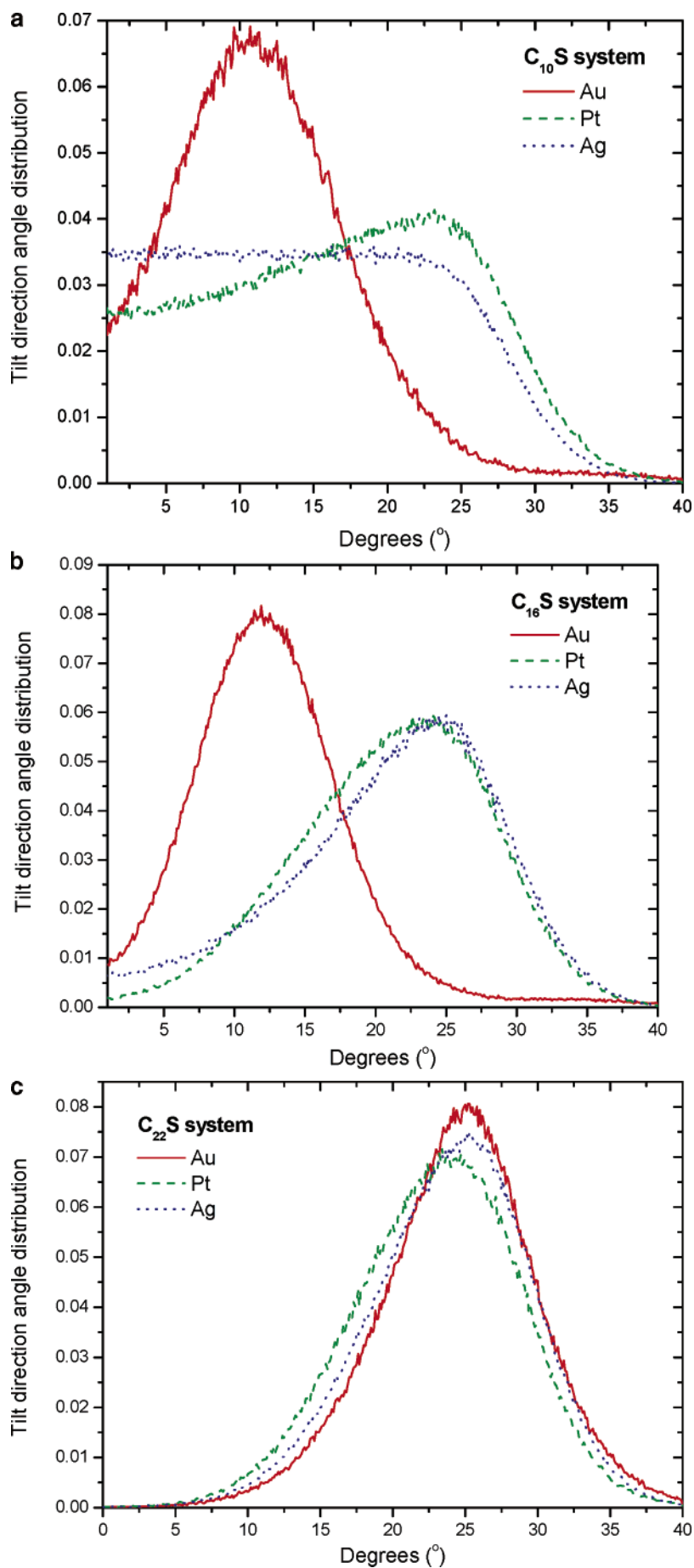


Figure 8. Distribution of the direction of molecular tilt, θ_m , at the end of the MC run as a function of the metal surface for the (a) $CH_3-(CH_2)_9-SH$, (b) $CH_3-(CH_2)_{15}-SH$, and (c) $CH_3-(CH_2)_{21}-SH$ systems.

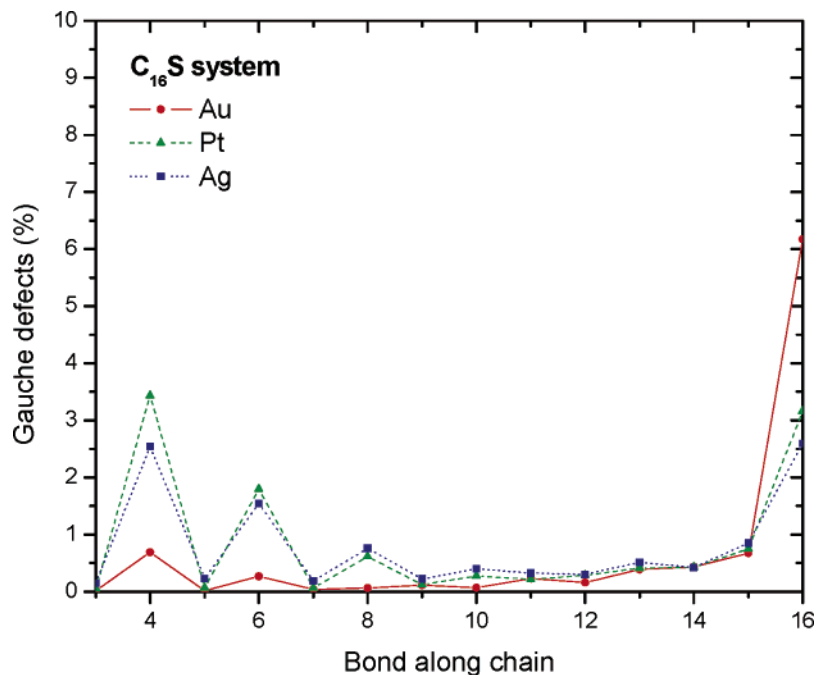


Figure 9. Percentage of bonds in the gauche configuration for dihedral angles along the adsorbed $C_{16}S$ chains on the three different metals. The first dihedral angle coincides with the third bond and involves the S headgroups.

in the alkanethiol chain and driving the two neighboring to the trimer atoms through a change in the pertinent dihedral angles. Given the new positions of the two driven atoms, a new trimer is constructed between them in such a way that the bonds of the altered segment preserve their equilibrium lengths. A more detailed description of the MC algorithm will be presented elsewhere.²⁴

The systems used in our classical simulations consisted of 110 alkanethiol molecules ($S-C_n-H_{2n+1}$) whose adsorption on the three metal substrates (Au, Ag, and Pt) was studied for three different chain lengths, equal to $n = 10, 16,$ and $22,$ respectively. The initial configuration is the one in which the S atoms are arranged in a hexagonal lattice and the molecules adopted an all-trans configuration with the planes of the C backbones in a herringbone arrangement. The alkanethiol chains were arranged in an orthorhombic simulation box with different dimensions $L_x, L_y,$ and L_z along the $x, y,$ and z directions, with periodic boundary conditions being applied only in the surface plane. The L_x and L_y values were different for each metal surface; on the basis of the experimental information about the molecular ordering of the S atoms on each one of the three substrates, the L_x and L_y dimensions were calculated to comply with the corresponding packing ($(\sqrt{3} \times \sqrt{3})R30^\circ$ for Au and Pt, and $(\sqrt{7} \times \sqrt{7})R10.9^\circ$ for Ag) and for a given lattice spacing. A summary of all simulated systems is given in Table 3. All simulations were carried out at the temperature $T = 300$ K in the canonical (NVT) statistical ensemble.

The simulations were executed until all properties of the systems under study were observed to fluctuate around a constant average value characteristic of a system at the state of thermodynamic equilibrium. The next step was to average over a large number of fully relaxed accumulated configurations to accurately predict their structural and conformational properties as a function of metal surface and chain length. The properties that are of interest in this work are the ones defining the molecular orientation of the alkanethiol self-assembled monolayer, namely, the tilt angle (θ_m), the tilt direction or precession angle (χ), the thickness of the monolayer, and the percentage

of gauche defects near the chain ends. We discuss all of them in detail in the next section.

C. Results and Discussion

System Equilibration. As an indication of the system equilibration, we plot in Figure 4 the time evolution (in MC steps) of the tilt angle as a function of the number of MC iterations for the $C_{16}S$ system for the three different substrates that were used in our MC simulations. It is obvious that the tilt angle for each one of the three systems ($C_{16}S/Au, C_{16}S/Ag, C_{16}S/Pt$) has reached its equilibrium value in the course of the MC run and thus can be calculated accurately by averaging over the accumulated configurations in the equilibrated regime. The same trend was observed for the rest of the structural properties examined here. A typical example of the final configuration for the $S-C_{16}-H_{33}$ system on the Au(111) substrate is shown in Figure 5 (side view).

Mean Atom Height and Monolayer Thickness (z_{tail}). The average atomic distances of a $C_{16}S$ chain from the three different surfaces is depicted in Figure 6. In all cases, the averaged z distance is observed to vary linearly with atom ranking number, typical of a fully extended chain conformation in the formed monolayer. The fact that R-SH chains on Ag appear to be more stretched than on Pt and especially on Au is directly related to the different tilt angle characterizing the simulated systems in the three cases, as discussed in more detail below. Also, irrespective of the chain length, the z distance of the last CH_3 group in the chain indicates a thicker monolayer for the film formed on the Ag substrate. The average $\langle z_{tail} \rangle$ values for all of the simulated systems are summarized in Table 4 and are fully consistent with the available experimental data^{4,8,40-42} for the same chain lengths and substrates. Noteworthy in the data of Table 4 is the relatively wide range of the reported experimental data for $\langle z_{tail} \rangle$ for SAMs adsorbed on the Au(111) surface.

Metal Surface Dependence of Tilt Angle (θ_m). Table 4 lists the average values of the molecular tilt angle, θ_m , for all nine simulated systems. The tilt angle follows the same trend

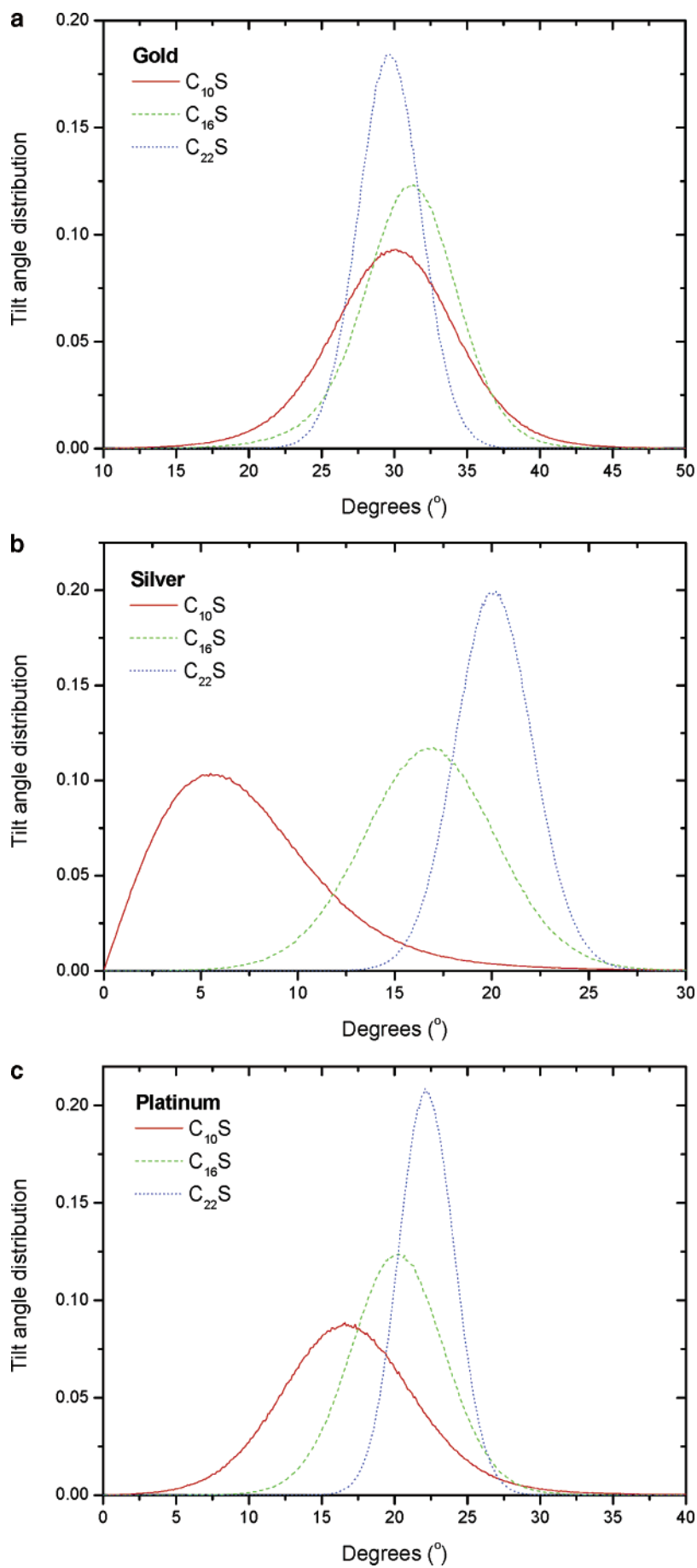


Figure 10. Normalized distributions of the collective molecular tilt as a function of chain length for the (a) Au, (b) Ag, and (c) Pt surfaces.

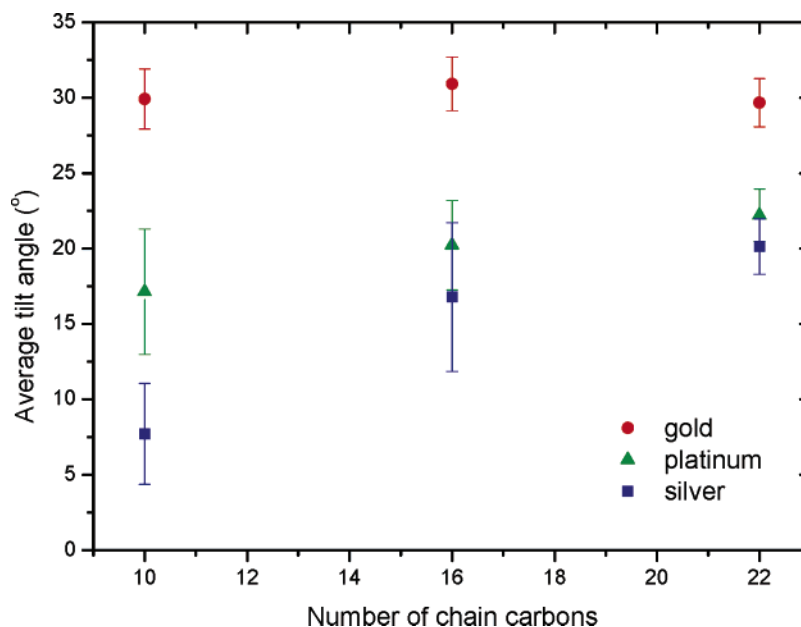


Figure 11. Average molecular tilt values as a function of chain length and substrate type.

irrespective of the type of the metal substrate and/or the molecular length of the system; the alkanethiol monolayers formed on the Ag substrate tilt less than those formed on the Pt or Au ones (30.9° for Au, 20.2° for Pt, and 16.8° for Ag on average). This is also shown in Figure 7, where the normalized distributions of the tilt angle for the $C_{16}S$ system are presented for all three metal surfaces. As expected, the tilt angle follows a normal distribution, which is consistent with the interplay of chain packing and S–metal interaction: an increase of the lattice spacing (going from Ag, to Pt, to Au) leads to a less dense packing of the monolayer and thus to higher tilting of the R–SH chains.

Tilt Direction (Precession) Angle (χ). Figure 8 shows the normalized distributions of the precession angle (χ) obtained from the MC simulations for the three metal substrates: Part a corresponds to the $C_{10}S$ system, part b to the $C_{16}S$ system, and part c to the $C_{22}S$ system. Tilt direction angles can be defined with respect to the nearest neighbor (NN) or next nearest neighbor (NNN) vectors (see Figure 1a). In this work, we define χ as the angle formed by the projection of the chain end-to-end vector on the surface with respect to the NN direction vector (Figure 2). For a perfect two-dimensional hexagonal lattice, one expects it to fluctuate in the interval between 0 and 30° with the two boundaries corresponding to the nearest and next nearest neighbor cases, respectively. Taking into account this notation, it is obvious from Figure 8 that the various systems do not display the same behavior, especially the shorter ones: there is a clear preference (see Figure 8b and c) for the alkanethiol SAMs formed on Ag and Pt substrates to tilt toward the next nearest neighbor ($\chi \approx 25^\circ$), which increases slightly as the molecular length increases. Alternatively, there are different aspects characterizing the behavior of tilt angle direction on the Au surface, as can be seen in Figure 8a and b, for the two smaller molecular lengths ($C_{10}S$ and $C_{16}S$), alkanethiols on Au tilt toward the nearest neighbor ($\chi \approx 10^\circ$); however, as their length increases, chains show a strong tendency to orient toward the next-nearest-neighbor direction ($\chi \approx 25^\circ$). This trend has also been observed in experimental measurements.¹ Summarized in Table 4 are the average values of the precession angles for all of the systems studied in the present work. It is also interesting to observe (compare, for example, the tilt direction graphs in Figure 8a to c) that for the shorter systems ($C_{10}S$ and

$C_{16}S$) the distributions of the tilt angle on the Pt and Ag metal surfaces are broader than those on the Au one, reflecting a smaller degree of uniformity of the tilt structure for these substrates. As the chain length increases, the distributions become less broad; that is, the uniformity increases.

Gauche Defects for Different Metal Surfaces. To determine whether or not the alkanethiol molecules are predominantly in the all-trans configuration, we investigated the percentage of gauche defects as a function of bond ranking number along the R–SH chains. One would expect that most of the defects would occur in the last bond because the methyl tail group has more freedom of rotation compared to the internal atoms. This was indeed observed to be the case for all simulated systems. In Figure 9, for example, we show the distribution of gauche defects along a $C_{16}S$ chain and how it varies with changing the metal surface. In fact, one can observe an oscillation in the fraction of the gauche defects between a maximum and minimum value for every other bond. This kind of arrangement among a system of densely packed molecules is energetically favorable over a random distribution of trans and gauche defects because it leads to conformations with no overlaps between neighboring molecules and it has also been observed elsewhere.^{17,19} In all cases, the percentage of gauche defects is very small (at most 4%) for all bonds, except the last one. The higher gauche defects of the first even-numbered bonds (mainly the fourth and the sixth ones) compared to the rest of the bonds is expected due to the constrained metal–S–CH₂ bond-bending angle, which makes it more difficult for these bonds to be in the trans state. However, a clear quantitative difference is observed between the different substrates for the defects of the last bond. For the Au surface, the percentage of gauche defects is larger (around 6.3%) than that for the Pt and Ag ones (around 2.5–3%). This is directly related to the different values of the S–S lattice spacing constant; that is, a larger S–S distance for the Au substrates leads to more free volume in the system and to higher probability of the gauche states for the last bond.

Chain Length Dependence of the Tilt Angle (θ_m). The distributions of the tilt angle, θ_m , are presented schematically in Figures 10 and 11; the latter shows the chain length dependence of the average tilt angle for all studied systems. There is a striking difference in the variation of the tilt angle with molecular length for the case of the Au surface compared

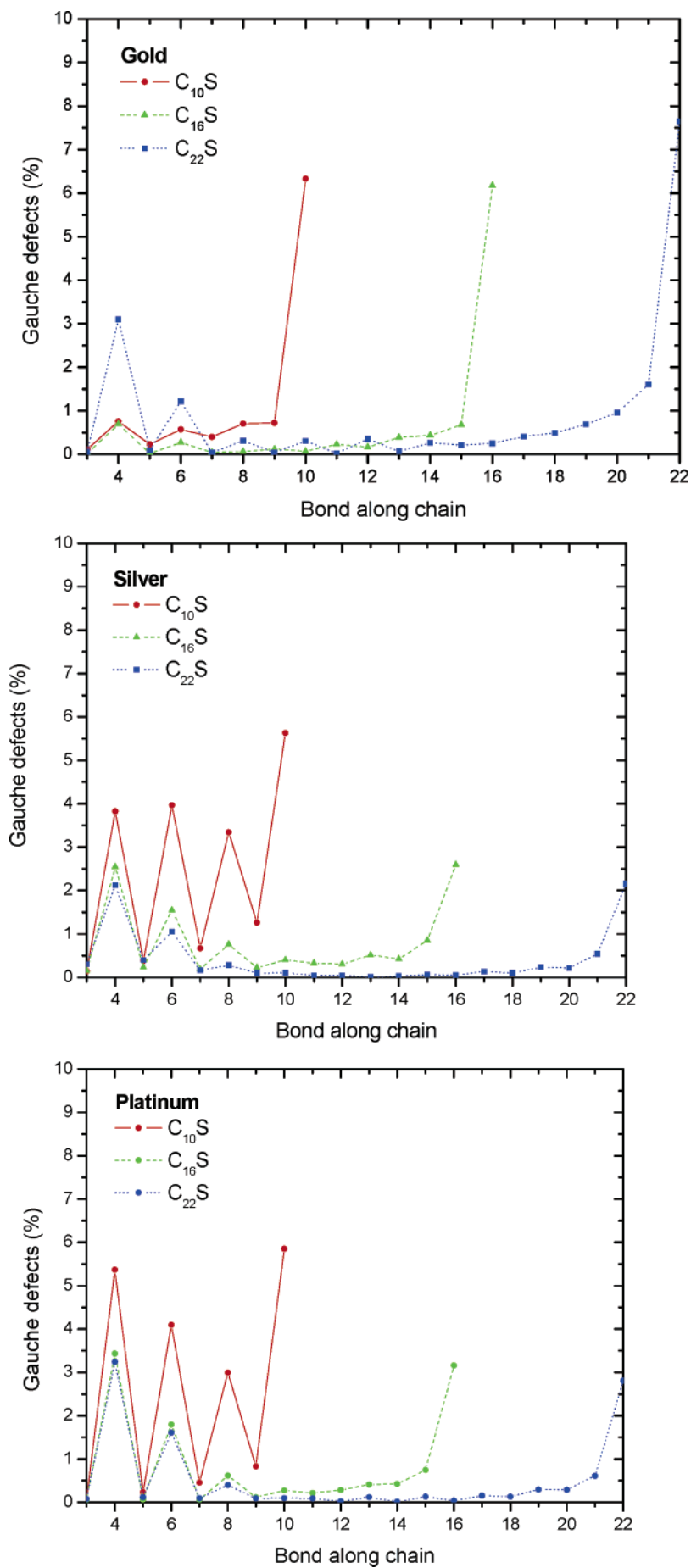


Figure 12. Percentage of gauche defects along an alkanethiol chain for various chain sizes on the (a) Au, (b) Ag, and (c) Pt substrates.

to the other two (Ag and Pt): As can be seen both from Figures 10b, 10c, and 11 and from the average values of θ_m in Table 4, the tilt angle increases as the chain length increases for Ag and Pt. This chain length dependence of the tilt structure reflects the competition between interchain forces, which, for a fixed substrate type, are increased with increasing chain length. On the other hand, the behavior of the tilt angle on Au is more complex: the tilt angle does not change dramatically with increasing molecular length as for the case of silver and platinum surfaces. It is also interesting that, overall, all three systems ($C_{10}S$, $C_{16}S$, and $C_{22}S$ on the gold substrate) exhibit very similar tilt angle values (around 30°). Experimentally, as far as the Au surface is concerned, the tilt angle is found to vary from 33 to 29° as the chain length increases from 10 to 25 carbon atoms.¹ To the best of our knowledge, there is no experimental information about the tilt angle dependence on chain length for the other two substrates (Ag and Pt).

Gauche Defects for Different Chain Lengths. Parts a–c of Figure 12 show the fraction of gauche defects as a function of the length of the R–SH molecule on the three substrates. The trend is similar to that of the tilt angle structure. Focusing in particular on the first three even-numbered bonds (fourth, sixth, and eighth), one can notice that above the Ag and Pt surfaces the fraction of gauche defects decreases with increasing molecular length, which does not seem to be the case for the chains above the Au surface where the larger $C_{22}S$ system exhibits the highest percentage of gauche defects for these bonds.

D. Conclusions

We have reported results from classical simulations concerning the structure of alkanethiol-based SAMs on three different metal surfaces (Au, Ag, and Pt); the molecule–surface force field was parametrized by quantum first-principles calculations. We have addressed for the first time issues related to the effects that the type of metal substrate can have on the structure and conformation of the adsorbed monomolecular film.

We found that the molecular tilt angle is different for the different substrates. The tilt structure on the Au surface is lamellar-like compared to that on Pt and (especially) Ag, where the alkanethiol molecules are typically standing normal to the surface (6° for the $C_{10}S$ system) reflecting a brush-like structure. The tilt direction is found to be more uniform in the case of the Au surface, particularly for the shorter chain length systems. This behavior changes for the largest molecular length ($C_{22}S$) where the same degree of uniformity is observed above all substrates. In addition, the tilt direction on the Au surface exhibits a transition from the NN to the NNN direction as the chain length increases from 10 or 16 carbon atoms to 22 carbon atoms. This behavior was not observed in the case of the Pt or Ag substrate. Differences in the chain length dependence of the structural properties on the three substrates are mainly related to the different equilibrium values to which the first metal–S–CH₂ angles are restricted in the classical simulations through the applied bond bending potential and their interplay with the intermolecular interactions between side chains; the latter become more important as the chain length increases or as the S–S lattice spacing on the surface decreases.

The information provided in this paper can in fact be very important for experimental purposes and the design of SAM structures with tailored properties because by selectively modifying the type of the substrate one can tune the properties of the resulting film toward the desired values. To this direction, SAMs present quite attractive features because they can be

utilized in order to attach different kinds of molecules above a metal surface (e.g., to immobilize biomolecules) by altering the functional endgroup while simultaneously initiating the growth of the adlayer toward a structure with, for example, a certain molecular orientation. In addition, if we take into account the quantum-based parametrization of our classical modeling approach, and also the very good agreement with the experimental data, then this simulation methodology can be used as a modeling tool for predicting properties of SAMs systems, for different chain lengths, temperatures, and substrates.

Acknowledgment. We are grateful to R. Caputo and L. M. Ghiringhelli for helping us with the ab initio calculations. Very fruitful discussions with N. van der Vegt and M. Praprotnik are greatly appreciated. O.A. acknowledges the funding of the international Max Planck Research School as well as the financial support provided by the PENED 2001 (code no. 01ED587) Greek National Programme.

References and Notes

- Schreiber, F. *Prog. Surf. Sci.* **2000**, *65*, 151.
- Ulman, A. *Chem. Rev.* **1996**, *96*, 1533.
- Strong, L.; Whitesides, G. M. *Langmuir* **1988**, *4*, 546.
- Chidsey, C. E. D.; Loiacono, D. N. *Langmuir* **1990**, *6*, 682.
- Nuzzo, R. G.; Dubois, L. H.; Allara, D. L. *J. Am. Chem. Soc.* **1990**, *112*, 558.
- Porter, M. D.; Bright, T. B.; Allara, D. L.; Chidsey, C. E. D. *J. Am. Chem. Soc.* **1987**, *109*, 3559.
- Fenter, P.; Eberhardt, A.; Liang, K. S.; Eisenberger, P. *J. Chem. Phys.* **1997**, *106*, 1600.
- Laibinis, P. E.; Whitesides, G. M.; Allara, D. L.; Tao, Y.; Parikh, A. N.; Nuzzo, R. G. *J. Am. Chem. Soc.* **1991**, *113*, 7152.
- Camillone, N., III; Chidsey, C. E. D.; Liu, G. Y.; Scoles, G. J. *Chem. Phys.* **1993**, *98*, 3503.
- Poirier, G. E.; Tarlov, M. J. *Langmuir* **1994**, *10*, 2853.
- Sellers, H.; Ulman, A.; Shnidman, Y.; Eilers, J. E. *J. Am. Chem. Soc.* **1993**, *115*, 9389.
- Harris, A. L.; Rothberg, L.; Dubois, L. H.; Levinos, N. J.; Dhar, L. *Phys. Rev. Lett.* **1990**, *64*, 2086.
- Fenter, P.; Eisenberger, P.; Li, J.; Camillone, N.; Bernasek, S.; Scoles, G.; Ramanarayanan, T. A.; Liang, K. S. *Langmuir* **1991**, *7*, 2013.
- Dhirani, A.; Hines, M. A.; Fisher, A. J.; Ismail, O.; Guyot-Sionnest, P. *Langmuir* **1995**, *11*, 2609.
- Kim, S. S.; Kim, Y.; Kim, H. I.; Lee, S. H.; Lee, T. R.; Perry, S. S.; Rabalais, J. W. *J. Chem. Phys.* **1998**, *109*, 9574.
- Yang, Y.; Yen, Y.; Ou Yang, L.; Yau, S.; Itaya, K. *Langmuir* **2004**, *20*, 10030.
- Hautman, J.; Klein, M. L. *J. Chem. Phys.* **1989**, *91*, 4994.
- Hautman, J.; Klein, M. L. *J. Chem. Phys.* **1990**, *93*, 7483.
- Mar, W.; Klein, M. L. *Langmuir* **1994**, *10*, 188.
- Bhatia, R.; Garrison, B. J. *Langmuir* **1997**, *13*, 4038.
- Li, T. W.; Chao, I.; Tao, Y. T. *J. Phys. Chem. B* **1998**, *102*, 2935.
- Siepmann, J. I.; McDonald, I. R. *Langmuir* **1993**, *9*, 2351.
- Shevade, A. V.; Zhou, J.; Zin, M. T.; Jiang, S. *Langmuir* **2001**, *17*, 7566.
- Alexiadis, O.; Daoulas, K. C.; Mavrantzas, V. G., to be submitted for publication.
- Yourdshahyan, Y.; Rappe, A. M. *J. Chem. Phys.* **2002**, *117*, 825.
- Fischer, D.; Curioni, A.; Andreoni, W. *Langmuir* **2003**, *19*, 3567.
- Franzen, S. *Chem. Phys. Lett.* **2003**, *381*, 315.
- Cometto, F. P.; Paredes-Olivera, P.; Macagno, V. A.; Patrio, E. *M. J. Phys. Chem. B* **2005**, *109*, 21737.
- Ghiringhelli, L. M.; Caputo, R.; Delle Site, L. *J. Phys.: Condens. Matter*, in press.
- Sellers, H.; Ulman, A.; Shnidman, Y.; Eilers, J. E. *J. Am. Chem. Soc.* **1993**, *115*, 9389.
- Beardmore, K. M.; Kress, J. D.; Gronbeck-Jensen, N.; Bishop, A. R. *Chem. Phys. Lett.* **1998**, *286*, 40.
- Zhang, L.; Goddard, W. A., III; Jiang, S. *J. Chem. Phys.* **2002**, *117*, 7342.
- Alavi, A.; Kohanoff, J.; Parrinello, M.; Frenkel, D. *Phys. Rev. Lett.* **1994**, *73*, 2599.

(34) We used version 3.4.1 of the CPMD code. Hutter J. et al. *CPMD*; copyright MPI für Festkörperforschung and IBM Zurich Research Laboratory 1995–1999.

(35) Perdew, J. P.; Burke, K.; Ernzerhof, M. *Phys. Rev. Lett.* **1996**, *77*, 3865.

(36) Rosenbluth, M. N.; Rosenbluth, A. W. *J. Chem. Phys.* **1955**, *23*, 356.

(37) De Pablo, J. J.; Laso, M.; Suter, U. W. *J. Chem. Phys.* **1991**, *96*, 2395.

(38) Dodd, L. R.; Boone, T. D.; Theodorou, D. N. *Mol. Phys.* **1993**, *78*, 961.

(39) Pant, P. V. K.; Theodorou, D. N. *Macromolecules* **1995**, *28*, 7224.

(40) Li, Z.; Chang, S.; Williams, R. S. *Langmuir* **2003**, *19*, 6744.

(41) Petrovykh, D. Y.; Kimura-Suda, H.; Opdahl, A.; Richter, L. J.; Tarlov, M. J.; Whitman, L. J. *Langmuir* **2006**, *22*, 2578.

(42) Bain, C. D.; Troughton, E. B.; Tao, Yu-Tai.; Evall, J.; Whitesides, G. M.; Nuzzo, R. G. *J. Am. Chem. Soc.* **1989**, *111*, 321.